Suppression of direct-transition phonon side bands in the magnetoluminescence from doped quantum wells

1996 J. Phys.: Condens. Matter 8 L363

(http://iopscience.iop.org/0953-8984/8/25/002)

J. Phys.: Condens. Matter **8** (1996) L363–L369. Printed in the UK

LETTER TO THE EDITOR

Suppression of direct-transition phonon side bands in the magnetoluminescence from doped quantum wells

S K Lyo, E D Jones and J F Klem

Sandia National Laboratories, Albuquerque, NM 87185, USA

Received 4 March 1996

Abstract. We present a theory for and the observation of LO-phonon side bands for transitions between the electron and hole Landau levels ($n_e, n_h = 0, 1, \ldots$). The side band of the primary $n_e = 0 \rightarrow n_h = 0$ line in an n-GaAs/InGaAs/AlGaAs quantum well is absent at low temperatures. The side bands of the secondary $n_e\ (>0) \rightarrow n_h = 0$ lines are relatively strong, growing with n_e in excellent agreement with the theory. The suppression of small-Δn ($=|n_e - n_h|$) side bands is due to the interference between the electron–phonon and hole–phonon recombination channels and the magnetic quantization in two dimensions.

Landau-level spectroscopy offers a powerful probe of electronic structures and interactions in semiconductor quantum wells (QWs) and heterostructures [1, 2]. A cw laser creates electrons and holes, for example, in n-doped degenerate QWs. The electrons thermalize rapidly into the Fermi–Dirac distribution in the conduction band, while the minority holes relax to near the top of the valence band according to the Boltzmann distribution. In a magnetic field $\boldsymbol{B} \| \boldsymbol{z}$ perpendicular to the QW plane, the carriers are quantized into the Landau levels ($n_e, n_h = 0, 1, \ldots$). Zero-phonon electron–hole recombinations $n_e \rightarrow n_h$ occur through direct transitions with $n_e = n_h$ or through weaker indirect off-diagonal transitions with $n_e \neq n_h$ in direct-gap QWs. At low temperatures with most of the holes in the ground level $n_h = 0$, the selection-rule-allowed $0 \rightarrow 0$ transition is dominant, while the zeroth-order forbidden $n_e\ (>0) \rightarrow 0$ transitions are weaker [2]. At high temperatures with higher hole levels populated, recombinations occur through the allowed direct transitions. This crossover between off-diagonal and direct transitions was utilized to determine the conduction and valence band energy dispersion curves [3].

In this letter, we present the first—to the best of our knowledge—observation of, and a microscopic theory for the longitudinal-optical- (LO-) phonon side bands of the band-to-band Landau-level spectra. Contrary to intuition, the side band of the primary $0 \rightarrow 0$ transition is found to be absent from an n-type $GaAs/In_{0.15}Ga_{0.85}As/Al_{0.15}Ga_{0.85}As$ (sample No 1) QW, while the side bands of the subsidiary $n_e\ (>0) \rightarrow 0$ lines are relatively strong and grow stronger with increasing n_e in excellent agreement with the theory. We will show that the inversion of the relative intensities arises from the interference between the electron–phonon and hole–phonon recombination channels in the presence of the magnetic quantization in two dimensions (2D). While the data to be presented here are restricted to a single sample, we have observed similar effects in a variety of configurations of InGaAs on GaAs including GaAs/InGaAs/GaAs.

The 4 K photoluminescence (PL) spectra from an n-type QW 80 Å wide (sample No 1: electron density $N_{2D} = 8.6 \times 10^{11}$ cm^{-2}) at 5 T are shown in figure 1(a). The

0953-8984/96/250363+07$19.50

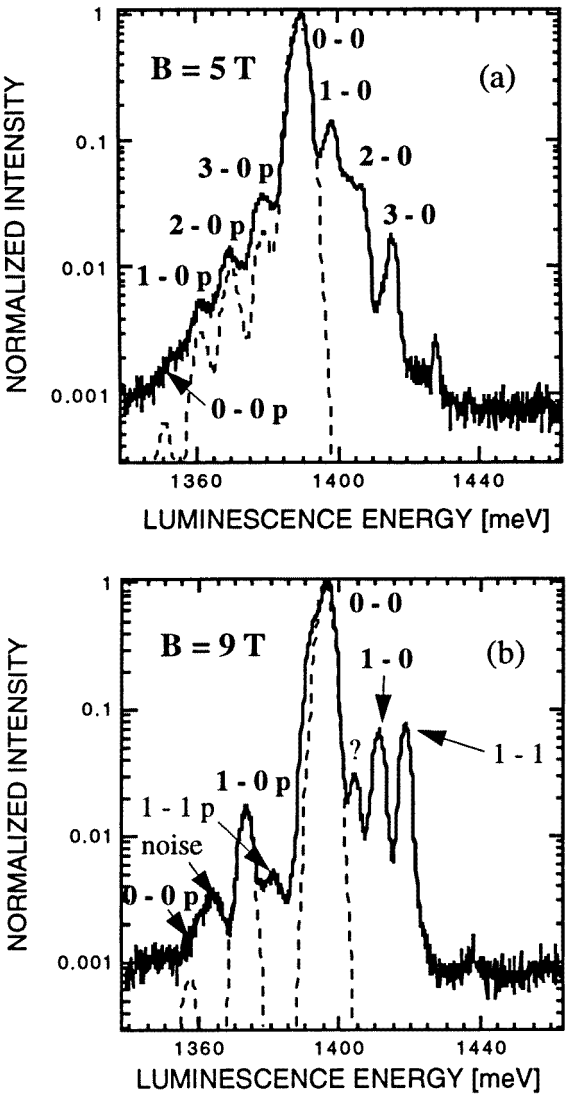

Figure 1. The 4 K PL spectra at (a) 5 T and (b) 9 T for sample No 1 excited with an argon-ion laser (514.2 nm) source. The spectral resolution is 1 meV. The $0 \rightarrow 0$ peak energies are 1390 and 1396 meV for 5 T and 9 T, respectively. The peak energies of side band '$n_e \rightarrow 0$p' are about 37 meV below the $n_e \rightarrow 0$ zero-phonon peaks. The calculated oscillator strengths are spread out into Gaussian line shapes (dashed curves) with a full width at half-maximum of 4 meV. The $1 \rightarrow 1$ and $1 \rightarrow 1$p peaks in (b) are from unrelaxed holes in the $n_h = 1$ level. The position of the peaks identified here rises nearly linearly with the field.

experimental technique is adequately described by Jones and Wickstrom [4]. In this strained QW, the light-hole state (i.e., $|3/2, \pm 1/2\rangle$) lies about 50 meV below the heavy-hole state (i.e., $|3/2, \pm 3/2\rangle$) (with light in-plane mass) due to compression. Therefore, only the $|3/2, \pm 3/2\rangle$ holes are relevant. The minority holes are mostly in the ground level $n_h = 0$. The zero-phonon lines consist of the primary $0 \rightarrow 0$ peak at 1390 meV and higher-

energy secondary $1 \rightarrow 0, 2 \rightarrow 0,$ and $3 \rightarrow 0$ peaks evenly separated by the electron cyclotron energy. The top $n_e = 3$ level is half-filled, neglecting spin splitting. Each of the n_e $(>0) \rightarrow 0$ peaks has a LO-phonon side band about 37 meV (close to the well-known GaAs LO-phonon energy 36.2 meV) below the peak and is labelled as '$n_e \rightarrow 0$p' in figure 1(a). It is important to note that the intensity of the side bands is *inverted* in relative strength, increasing with n_e. In particular, the side band of the prominent $0 \rightarrow 0$ line is *absent*. A similar behaviour is displayed at 9 T in figure 1(b) where the top level, $n_e = 1$, is filled.

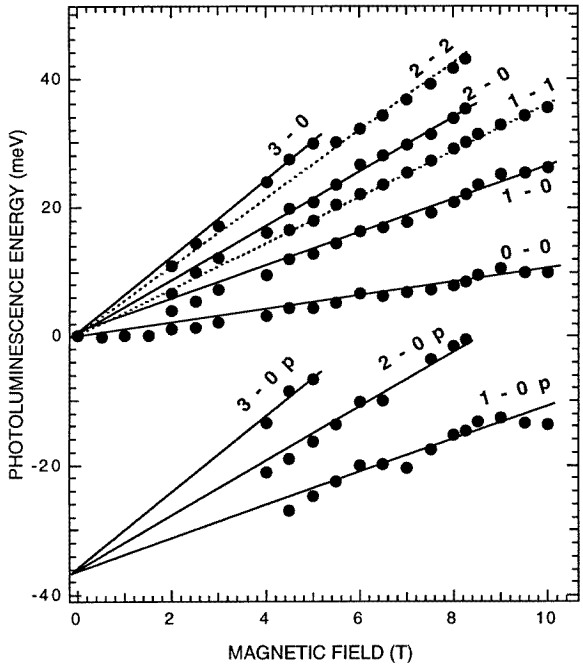

Figure 2. The 4 K PL peaks for sample No 1 as a function of *B*. The zero energy is at 1385.8 meV. The lines are guides to the eye. The lines for the side bands are displaced from the zero-phonon counterparts by about 37 meV. Only the PL peaks which move with *B* are shown. Weak 1–1p transitions which appear above 7.8 T are not shown. The data along the dotted lines are due to the hot holes.

The peak PL energies are displayed as a function of *B* in figure 2. The solid lines (which are guides to the eye) for the *n*–0p phonon side bands are about 37 meV below but parallel to those for *n*–0 zero-phonon transitions ($n = 1, 2, 3$). The data along the dotted lines for the 1–1 and 2–2 transitions are due to hot holes. Various unidentified *B*-independent peaks such as those labelled 'noise' or '?' in figure 1(b) are not shown. The authors are not aware of any previous observation of the phonon side bands from band-to-band transitions in QWs, although phonon side bands were observed earlier from exciton luminescence [5] and phonon-assisted lasing [6]. We have not seen side bands in GaAs/AlGaAs. In this lattice-matched system, there is no large strain-induced contribution to the heavy–light-hole splitting and hence, because of the small splitting due to the confinement effect alone, the spectral lines are harder to resolve.

In the following, we present a theory of the phonon side bands to explain the data. For zero-phonon transitions, we consider only the total intensity of the $0 \rightarrow 0$ transition,

neglecting the impurity interactions. The low-T line width and the off-diagonal transitions are caused by carrier–impurity interactions and are well understood [7]. We calculate the total intensity of each side band with zero width (i.e., ignoring impurity interactions) and compare with the $0 \rightarrow 0$ intensity. The effect of the line width is considered only phenomenologically at the end to compare the theory and the data. We are interested in the low-carrier-density and the low-T regime where the carriers are in the ground sublevels.

A system of electrons and holes interacting with the LO phonons is described, in the Landau gauge, by the Fröhlich Hamiltonian [8]

$$H = \sum_{\alpha,t} \varepsilon_{\alpha n} a^{\dagger}_{\alpha t} a_{\alpha t} + \sum_{\boldsymbol{q}} \hbar\omega_{\boldsymbol{q}} b^{\dagger}_{\boldsymbol{q}} b_{\boldsymbol{q}} + \sum_{\alpha,t,t',\boldsymbol{q}} V^{\alpha}_{t,t'}(\boldsymbol{q}) a^{\dagger}_{\alpha t'} a_{\alpha t} (b_{\boldsymbol{q}} + b^{\dagger}_{-\boldsymbol{q}}) \tag{1}$$

where $t = (n, k_y)$ and k_y is the wave number. The first term in (1) is the Hamiltonian for the electrons and the holes in the nth level with the energy

$$\varepsilon_{\alpha n} = \left(n + \frac{1}{2}\right)\hbar\omega_{\alpha}. \tag{2}$$

In (1), $a^{\dagger}_{\alpha t}, a_{\alpha t}$ are the fermion creation and annihilation operators, and $\omega_a = eB/m_{\alpha}c$, where m_{α} indicates the electron (m_{e}) and hole (m_{h}) effective masses. The second term in (1) is the LO-phonon Hamiltonian, where $b^{\dagger}_{\boldsymbol{q}}, b_{\boldsymbol{q}}$ are the boson creation and annihilation operators. The dispersion of the frequency will be ignored in the numerical evaluation (i.e., $\hbar\omega_{\boldsymbol{q}} \simeq 37$ meV). Finally, the last term in (1) describes the carrier–LO-phonon interaction:

$$V^{\alpha}_{t,t'}(\boldsymbol{q}) = V_{\alpha\boldsymbol{q}} \delta_{k'_y, k_y + q_y} S_{\alpha}(q_z) \exp\left\{ \mathrm{i}\ell^2 \left(k_y q_x + \frac{1}{2} q_x q_y \right) + \mathrm{i}(n - n')\phi_{\boldsymbol{q}} \right\} \mathcal{J}_{nn'}\left(\frac{1}{2}\ell^2 q_{\parallel}^2 \right) \tag{3}$$

where $\ell = (eB/\hbar c)^{-1/2}$ and

$$V_{\alpha\boldsymbol{q}} = s_{\alpha} \left(\frac{4\pi\eta\hbar^{5/2}\omega_{\boldsymbol{q}}^{3/2}}{\Omega q^2 \sqrt{2m_{\alpha}}} \right)^{1/2}. \tag{4}$$

The quantities $q_{\parallel}, \phi_{\boldsymbol{q}},$ and $\mathcal{J}_{nn'}(x)$ in (3) are defined by $q_x + \mathrm{i}q_y = q_{\parallel} \exp(\mathrm{i}\phi_{\boldsymbol{q}})$ and

$$\mathcal{J}_{nn'}(x) = \sqrt{\frac{n_<!}{n_>!}} \mathrm{e}^{-x/2} x^{(n_> - n_<)/2} L_{n_<}^{n_> - n_<}(x) \tag{5}$$

where $L_{n_<}^{n_> - n_<}(x)$ is the associated Laguerre polynomial and $n_>$ ($n_<$) is the larger (lesser) of n and n'. In (4), Ω is the sample volume, and η is the dimensionless electron–phonon coupling constant. The sign of the interaction with the phonon field is opposite for the electrons and the holes (i.e., $s_{\mathrm{e}} = +1$ and $s_{\mathrm{h}} = -1$). Finally, $S_{\alpha}(q_z)$ is defined by

$$S_{\alpha}(q_z) = \int \phi_{\alpha}(z)^2 \Phi(q_z, z)\, \mathrm{d}z \tag{6}$$

where $\Phi(q_z, z)$ is the phonon field and $\phi_{\alpha}(z)$ is the ground-state confinement wave function.

The line-shape function is proportional to the one-phonon-assisted electron–hole recombination rate. Initially, we calculate this rate using a simple perturbation theory. The result is justified later by a rigorous dipole–dipole correlation function approach based on a temperature-ordered Green's function technique. The latter also helps to remove divergences and to include dielectric screening. The line-shape function is given in an arbitrary unit by

$$F_{\mathrm{ph}}(\omega) = \pi \sum_{t,t',\boldsymbol{q},\pm} |t^{\pm}_{\mathrm{e}t,\mathrm{h}t'}(\boldsymbol{q})|^2 f(\varepsilon_{\mathrm{e}n} - \mu_{\mathrm{e}}) f(\varepsilon_{\mathrm{h}n'} - \mu_{\mathrm{h}}) \delta(\hbar\omega - \varepsilon_{\mathrm{e}n} - \varepsilon_{\mathrm{h}n'} \pm \hbar\omega_{\boldsymbol{q}}) \tag{7a}$$

where the transition matrix $t_{et,ht'}$ equals

$$t^{\pm}_{et,ht'}(\boldsymbol{q}) = -d_{cv}\left(\frac{\tilde{V}^{e}_{t',t}(\boldsymbol{q})}{\varepsilon_{en'} - \varepsilon_{en} \pm \hbar\omega_{\boldsymbol{q}}} + \frac{\tilde{V}^{h}_{t',t}(\boldsymbol{q})}{\varepsilon_{hn} - \varepsilon_{hn'} \pm \hbar\omega_{\boldsymbol{q}}}\right)\sqrt{N_{\boldsymbol{q}} + \frac{1}{2} \pm \frac{1}{2}}. \tag{7b}$$

In (7), $\hbar\omega$ is the photon energy minus the band gap, $f(x) = (\exp(x/k_B T) + 1)^{-1}$, μ_e (μ_h) is the electron (hole) chemical potential, and $N_{\boldsymbol{q}}$ is the boson function. The quantity $\tilde{V}^{\alpha}_{t',t}(\boldsymbol{q})$ is given by (3) with $V_{\alpha\boldsymbol{q}}$ replaced by the screened carrier–phonon interaction $\tilde{V}_{\alpha\boldsymbol{q}}$, and d_{cv} ($\propto\langle\phi_e|\phi_h\rangle$) is the interband dipole matrix element connecting the conduction (c) and valence (v) band. The upper and lower signs correspond to the one-phonon emission and absorption processes, respectively.

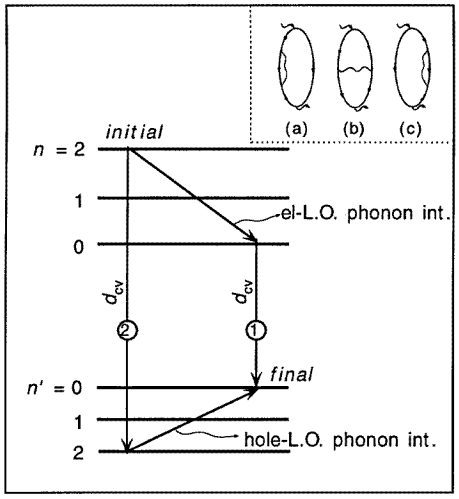

Figure 3. A two-step phonon-assisted recombination process whereby an electron in the initial level $n = 2$ falls into a hole at $n' = 0$. The vertical and slanted lines denote the dipolar coupling and the carrier–phonon scattering, respectively. The levels $n_e = 0$ and $n_h = 2$ are intermediate virtual states. The inset shows a diagrammatic representation: the solid lines on the left and right are dressed electron and hole propagators, respectively. Long curvy lines are the phonon propagators. The short wavy curves are the dipole-field vertices ($\propto d_{cv}$). The arrows denote the flow of energy.

A two-step phonon-assisted process recombining an electron in level n (=2) with a hole in n' (=0) is illustrated in figure 3. The first term in (7*b*) corresponds to channel 1 in figure 3 whereby an electron in the $n_e = n$ level is admixed with an intermediate virtual state $n_e = n''$ through electron–phonon interaction and then falls into a hole in the $n_h = n'$ level emitting a photon through d_{cv}. Similarly, the second term in (7*b*) corresponds to channel 2 where an electron in the $n_e = n$ level is coupled to an intermediate virtual state $n_h = n'''$ through d_{cv} and then falls into a hole at $n_h = n'$ through hole–phonon interaction. The dipole field couples only the electrons and holes with the same quantum number (i.e., $n = n''', n' = n''$). Here, it is convenient to use the electron picture for the valence band and then convert the result into the hole picture by reversing the signs of the electron energies as well as the electron–phonon interaction for the second term of (7*b*).

A microscopic justification for the result in (7) is provided by the dipole–dipole correlation function diagrams displayed in the inset of figure 3. A tedious evaluation [8] of these diagrams indicates that the two terms in (7*b*) should be replaced, apart from the

numerators $\tilde{V}^{\rm e}_{t',t}(\boldsymbol{q})$ and $\tilde{V}^{\rm h}_{t',t}(\boldsymbol{q})$, by the real parts of the electron and hole propagators $G_{{\rm e}n'}(\varepsilon_{{\rm e}n} - \mu_{\rm e} \mp \hbar\omega_{\boldsymbol{q}} + {\rm i}0)$ and $G_{{\rm h}n}(\varepsilon_{{\rm h}n'} - \mu_{\rm h} \mp \hbar\omega_{\boldsymbol{q}} + {\rm i}0)$, respectively. The divergence due to the vanishing denominators is therefore avoided by the damping of the energy levels. The imaginary parts of the same Green's functions yield resonant processes and are not of interest here: they contribute to the relaxation toward the thermal equilibrium through two-step processes whereby an electron (hole) relaxes from one level to another in the conduction (valence) band through resonant phonon emission or absorption and then recombines with a hole (electron) through a zero-phonon direct transition; we are not concerned with how the equilibrium is reached. The Green's function $G_{\alpha n}(z)$ is defined by the standard expression $G_{\alpha n}(z)^{-1} = z - \varepsilon_{\alpha n} + \mu_\alpha - \Sigma_{\alpha n}(z)$. The dominant contribution to the self-energy $\Sigma_{\alpha n}(z)$ arises, in doped QWs, from interactions with ionized dopant impurities [7]. The widths of spectral lines are determined by the imaginary part $\Gamma_{\alpha n}$ of $\Sigma_{\alpha n}$. The divergences mentioned above are relevant only in a very-high-density system (e.g., $N > 1.1 \times 10^{12}$ cm^{-2} in GaAs QWs) where the Fermi energy exceeds the LO-phonon energy. At lower densities, the expression in (7*b*) has no divergence problem even without damping. The first and third diagrams in the inset of figure 3 yield the first and second term alone in (7*b*) respectively, while the cross term arises from the diagram in the middle. The cross term corresponds to the interference between the channels 1 and 2 in figure 3 and is responsible for the absence of the $0 \rightarrow 0$ side band in the spectral lines in figures 1 and 2 as will be discussed later.

To gain an understanding of the suppression of the direct-transition side bands as well as for a numerical evaluation, we use the approximation $\phi_{\rm e}(z) \simeq \phi_{\rm h}(z)$ in the following for well-confined electrons and holes. Because the two denominators in (7*b*) are identical (i.e., $= \pm\hbar\omega_{\boldsymbol{q}}$) for $n = n'$, the quantity in the large parentheses of (7*b*) becomes proportional to $(\pm 1/\hbar\omega_{\boldsymbol{q}})(\tilde{V}_{{\rm h}\boldsymbol{q}} + \tilde{V}_{{\rm e}\boldsymbol{q}}) = (\pm 1/\hbar\omega_{\boldsymbol{q}})(V_{{\rm h}\boldsymbol{q}} + V_{{\rm e}\boldsymbol{q}})$, which is independent of the dielectric screening. The latter equality is valid in the random-phase approximation (RPA) [9] in the limit $\phi_{\rm e}(z) = \phi_{\rm h}(z)$ [10]. The intensities from the direct transitions are then proportional to $\xi \equiv (1 - (m_{\rm e}/m_{\rm h})^{1/4})^2$ since $V_{{\rm h}\boldsymbol{q}} = -V_{{\rm e}\boldsymbol{q}}(m_{\rm e}/m_{\rm h})^{1/4}$ and become very small as long as $m_{\rm h}$ is not much larger than $m_{\rm e} = 0.07m_0$. This is relevant to our sample, where the average in-plane hole mass $m_{\rm h} \simeq 0.14m_0$ is relatively light (compared with the bulk $m_{\rm h} \sim 0.45m_0$), yielding $\xi = 0.025 \ll 1$. The degree of the cancellation between the electron–phonon and hole–phonon channels decreases for increasing $\Delta n = |n - n'|$, resulting in a stronger intensity for larger Δn.

The low-temperature spectral intensities of the side bands are calculated for the phonon emission process in (7) for sample No 1 using the bulk GaAs electron–phonon coupling constant $\eta_{\rm GaAs} = 0.06$ [11] and are compared with the data in figure 1 at 9 T and 5 T, where the $n_{\rm e} = 1$ level is filled and the $n_{\rm e} = 3$ level is half-filled, respectively. An infinite-barrier approximation is employed for the confinement wave functions due to the negligible penetration of the electron and hole wave functions into the barriers. For sample No 1, the effect of phonon confinement is expected to be small for the low Al concentration $x = 0.15$ as in GaAs/Al$_x$Ga$_{1-x}$As QWs, where the confinement effect is important only above $x = 0.2$ [12]. Therefore, a bulk phonon model $\Phi(q_z, z) = \exp({\rm i}q_z z)$ is used for $S_\alpha(q_z)$ in (6). This approximation is also consistent with the fact that the phonon energy observed in figure 1 is that of the bulk phonons. Confined phonons have stronger interactions with the carriers, yielding stronger side bands. Formation of the confined phonon modes and the interface modes in layered *alloy* structures lacks a quantitative explanation at present. In figure 1, the dielectric screening is neglected for the dynamic screening at the optical phonon energy. The latter is not expected to be as efficient as the static screening, although it is not understood well currently [13]. The calculated intensity is spread out into a Gaussian line shape with a 4 meV full width at half-maximum for each side band. Otherwise, there are no adjustable

parameters. The basic features of the predictions of the theory show excellent agreement with the data. In order to demonstrate the cancellation between the two terms in (7*b*), the same calculation was repeated after changing the sign of the second term therein. The $0 \rightarrow 0$p strength increased drastically above the $1 \rightarrow 0$p peak—contrary to the data.

Although the $0 \rightarrow 0$p side band is considerably weaker than other side bands, its relative strength increases significantly at high fields because m_h increases with the energy of the $n_h = 0$ level due to the valence band nonparabolicity [3]. Although we have used an average hole mass $m_h \simeq 0.14m_0$ [3] in the field range of interest, the $n_h = 0$ hole mass becomes much larger than $0.14m_0$ at high fields, yielding an increasingly larger ξ. In contrast, m_e remains approximately constant. Our preliminary data show that the $0 \rightarrow 0$p intensity begins to be visible above 15 T due to this effect. In this regard, the weak but visible $1 \rightarrow 1$p peak at 9 T in figure 1(b) (much smaller than the $1 \rightarrow 0$p peak as predicted by our theory) can be attributed to this effect. The population of the $n_h = 1$ level is due to unrelaxed holes, which have large m_h ($>0.25m_0$) due to their large energy.

In summary, we have presented a microscopic theory for and the observation of LO-phonon side bands for the optical transitions between the electron and hole Landau levels from an n-type QW. The main feature of the data is that the intensity peaks of the phonon side bands are inverted in relative strength compared with those of the zero-phonon lines: the side band of the predominant $n_e = 0 \rightarrow n_h = 0$ transition is nearly absent while the side bands of the secondary n_e (>0) $\rightarrow n_h = 0$ lines are relatively strong, growing with n_e in excellent agreement with the theory. The suppression of small-Δn ($=|n_e - n_h|$) side bands arises from the interference between the electron–phonon and hole–phonon recombination channels and the magnetic quantization in 2D.

The authors thank P J Turley of Duke University for valuable conversations about the phonon confinement in quantum-well structures and D Emin for helpful discussions about electron–phonon interactions. This work was supported by US DOE under Contract No DE-AC04-94AL85000.

References

[1] Worlock J M, Maciel A C, Petrou A, Perry C H, Aggarwal R L, Smith M and Gossard A C 1984 *Surf. Sci.* **142** 486
[2] Lyo S K, Jones E D and Klem J F 1988 *Phys. Rev. Lett.* **61** 2265
[3] Jones E D, Lyo S K, Fritz I J, Klem J F, Schirber J E, Tigges C P and Drummond T J 1989 *Appl. Phys. Lett.* **54** 2227
[4] Jones E D and Wickstrom G L 1985 *Proc. SPIE (Southwest Conf. on Optics)* **540** 362
[5] Skolnick M S, Nash K J, Tapster P R, Mowbray D J, Bass S J and Pitt A D 1987 *Phys. Rev.* B **35** 5925
Von Lehmen A, Zucker J E, Heritage J P and Chemla D S 1987 *Phys. Rev.* B **35** 6479
[6] Holonyak N Jr 1980 *IEEE J. Quantum Electron.* **16** 170
Nam D W, Holonyak N Jr, Hsieh K C, Kuo C P, Fletcher R M, Osentowskie T D and Craford M G 1989 *Appl. Phys. Lett.* **54** 2446
[7] Lyo S K 1989 *Phys. Rev.* B **40** 8418
[8] Scher H and Holstein T 1966 *Phys. Rev.* **148** 598
[9] Ando T and Uemura Y J 1974 *J. Phys. Soc. Japan* **37** 1044
[10] Lyo S K and Jones E D, unpublished
[11] Brown F C 1962 *Polarons and Excitons* ed C G Kuper and G D Whitfield (New York: Plenum) p 323
Alloying with 15% of In does not change η significantly because $\eta_{GaAs} \sim \eta_{InAs} = 0.05$.
[12] Turley P J, private communication
[13] Ahn D 1994 *Phys. Rev.* B **50** 1713